REGULAR PAPER

CrossMark

Suppression of segregation of the phosphorus δ-doping layer in germanium by incorporation of carbon

Michihiro Yamada[1], Kentarou Sawano[2], Masashi Uematsu[1], Yasuo Shimizu[3], Koji Inoue[3], Yasuyoshi Nagai[3], and Kohei M. Itoh[1]*

[1]*School of Fundamental Science and Technology, Keio University, Yokohama 223-8522, Japan*
[2]*Advanced Research Laboratories, Tokyo City University, Setagaya, Tokyo 158-0082, Japan*
[3]*The Oarai Center, Institute for Materials Research, Tohoku University, Oarai, Ibaraki 311-1313, Japan*

*E-mail: kitoh@appi.keio.ac.jp

The successful formation of abrupt phosphorus (P) δ-doping profiles in germanium (Ge) is reported. When the P δ-doping layers were grown by molecular beam epitaxy (MBE) directly on Ge wafers whose surfaces had residual carbon impurities, more than a half the phosphorus atoms were confined successfully within a few nm of the initial doping position even after the growth of Ge capping layers on the top. On the other hand, the same P layers grown on Ge buffer layers that had much less carbon showed significantly broadened P concentration profiles. Current–voltage characteristics of Au/Ti/Ge capping/P δ-doping/n-Ge structures having the abrupt P δ-doping layers with carbon assistance showed excellent ohmic behaviors when P doses were higher than 1×10^{14} cm^{-2} and the capping layer thickness was as thin as 5 nm. Therefore, the insertion of carbon around the P doping layer is a useful way of realizing ultrashallow junctions in Ge. © 2016 The Japan Society of Applied Physics

1. Introduction

Germanium (Ge) has drawn much attention as a promising candidate for a next-generation channel material in metal oxide semiconductor field effect transistors (MOSFETs).[1] The realization of high-performance n-channel Ge MOSFETs requires the formation of Ohmic contacts with sufficiently low resistivity. In addition, the formation of an ultrashallow junction is required to avoid undesirable short channel effects (e.g., punch through).[1] The existence of large Schottky barriers (0.5–0.6 eV) against electrons for practically all kinds of metal contacts owing to Fermi level pinning was identified as one of the challenges.[2,3] This has been partially overcome by insertion of ultrathin insulators between the metal and Ge to alleviate Fermi level pinning.[4–9] However, such insertion of the insulator naturally leads to high contact resistance. More recently, NiGe alloy was identified as a promising metal for ohmic contacts when it is placed on highly doped Ge.[10–12] Therefore, the development of a high-concentration donor-doping method near the surface of Ge is needed to utilize the NiGe contact metal and also to achieve sufficient electron tunneling through the thin Schottky barriers to utilize other metals for the formation of the low-resistivity shallow contacts. The most conventional ion-implantation method requires post-implantation annealing, which leads to significant spatial broadening for the case of donors in Ge[13,14] because the diffusivities of n-type dopants in Ge are proportional to the square of the dopant concentration.[15–17] In the present work, we report the successful doping of Ge by phosphorus (P) up to the concentration 10^{19}–10^{20} cm^{-3} within a few nm in the depth direction. The δ-doping technique, i.e., the insertion of a sub-monolayer of donors in the epitaxial growth layer of Ge, was utilized. No postgrowth annealing was needed to achieve high activation in the δ-doping techniques.[18,19]

It has been well known that the donors in Ge tend to segregate towards the surface during the growth of further Ge on top of the P δ-layer.[18,19] Such segregation i) reduces the peak donor concentration and ii) broadens or smears out the dopant profiles in the depth direction. In the past, the

suppression of such segregation was achieved by lowering the growth temperature.[18–23] However, low growth temperatures also led to the degradation of the crystalline quality of the host semiconductor.[24] The present work utilizes the incorporation of carbon atoms around the δ-doping region to reduce the dopant segregation and allow the growth at 300 °C in order to achieve electronic contact current–voltage (I–V) characteristics desirable for the shallow-junction applications.

2. Experimental methods

The δ-doping of P during the growth of Ge was performed by molecular beam epitaxy (MBE) on nondoped Czochralski Ge(111) substrates having the resistivities of 30–40 Ω cm. After chemical cleaning with NH$_4$OH and HF to remove the native oxide, the substrates were loaded into the MBE chamber. A pregrowth annealing was performed at 700 °C for 10 min in ultrahigh vacuum ($\sim 10^{-10}$ Torr). It has been known that carbon is the dominant residual impurity on the surface of Ge substrates after chemical cleaning and preannealing in vacuum.[25] We use such residual carbon impurities to investigate the effect of carbon insertion, as shown schematically at the top left side of Fig. 1. P was directly deposited on the substrate with various concentrations using a GaP decomposition Knudsen cell, where the amount of Ga atoms are efficiently separated from the P beam within a special orifice plate on top of the cell.[26] In our experiments, the Ga contamination was below the secondary ion mass spectrometry (SIMS) detection limit (4×10^{14} cm^{-3}). After the P deposition, Ge capping layers of various thicknesses were grown with the constant growth rate of 0.5 Å/s at various growth temperatures in the range of 300–500 °C. In order to prepare the δ-doped P without carbon, we prepared the control samples in which Ge buffer layers were grown before the P δ-doping layers, as shown schematically at the top right side of Fig. 1. The buffer layers were grown with the same growth rate and growth temperature as for the capping layer. Here carbon atoms exist between the Ge substrate and the buffer layer but they do not reach the P δ-doped layer, as will be shown below by SIMS analysis. The growth conditions of eleven samples (labeled A–K) are summarized in Table I.

© 2016 The Japan Society of Applied Physics
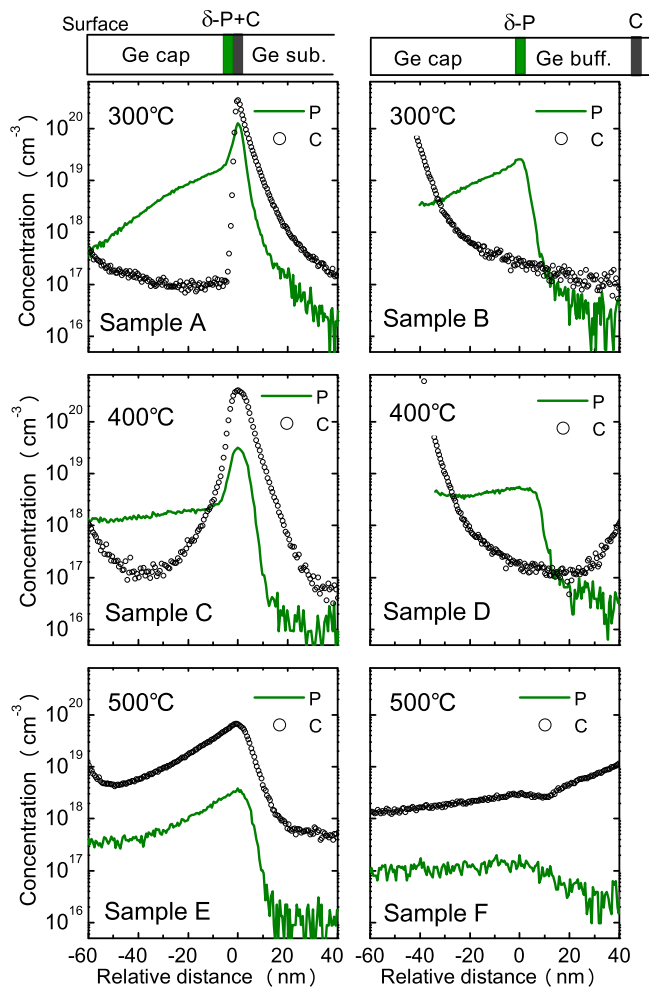
Fig. 1. (Color online) SIMS depth profiles of P and carbon for the δ-doped samples with 1×10^{14} cm^{-2} P on Ge(111) at growth temperatures from 300 to 500 °C. Samples A, C, and E include carbon atoms in the δ-doped layer, while samples B, D, and F do not. Zero in the relative distance is the initial doping position of δ-doped P.

Table I. Growth temperature, presence of carbon in the δ-doping layer, sheet density of P, and capping layer thickness for the samples. Ge(111) substrates are used for all samples.

| Sample name	Growth temperature (°C)	Presence of carbon	Sheet density of dopant (cm^{-2})	Capping layer thickness (nm)
A	300	Yes	1×10^{14}	≥40
B	300	No		
C	400	Yes		
D	400	No		
E	500	Yes		
F	500	No		
G	300	Yes	5×10^{13}	15
H	300	Yes	1×10^{14}	15
I	300	Yes	5×10^{14}	15
J	300	Yes	1×10^{14}	5
K	300	Yes	1×10^{14}	3

The depth distribution of P and carbon in these structures was measured by SIMS (PHI ADEPT1010) using Cs$^+$ primary ions with an acceleration energy of 1 keV. The interface between the substrate and the capping layer was observed by cross-sectional transmission electron microscopy (XTEM)

and atom probe tomography (APT). APT has proved to be a useful method for determining principal dopant distributions in Ge-based materials.[27,28] Here, the APT technique was used to obtain mass information on the regions around P δ-doped and carbon-incorporated layers. APT measurements were performed with a laser-assisted local electrode atom probe (Ametek LEAP4000XHR) equipped with a reflection lens to obtain a high mass resolution and a high signal-to-noise ratio. In the APT measurements, an ultraviolet laser (wavelength: 355 nm; power: 25 pJ) was used. The needle specimens were cooled down to 35 K to inhibit surface migration during ionization and extraction of the atoms from the needle-shaped specimen, and the pressure in the analysis chamber was around 2.0×10^{-11} Torr. The electric junction characteristics (I–V) were investigated by depositing Au/Ti to form Schottky diodes. Au/Ti pads of a diameter of 50 μm were defined by standard photolithography and were formed by vacuum deposition on the top of the HF-treated samples. Here, the thickness of the capping layers was reduced to 15 nm or less in order to enhance electron tunneling through the barrier to achieve Ohmic behaviors. AuSb alloys were deposited on the back of the samples with large area in order to obtain Ohmic contacts. In order to investigate the activation of δ-doped P, Hall measurements were performed at 3 K using Hall mesa structures with AuSb Ohmic contacts. The Hall bar has a length of 200 μm and a width of 400 μm.

3. Results and discussion

3.1 Observation of P segregation for structures with and without carbon
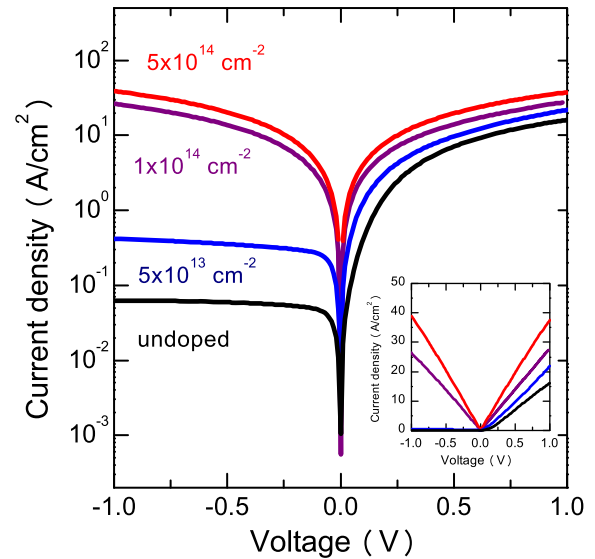
Figure 1 shows the SIMS depth profiles of P and carbon for samples A–F. The horizontal axis represents the relative distance from the P δ-doping position. In samples A, C, and E, the carbon concentration of higher than 10^{19} cm^{-3} exists around the P δ-doping layer (left side of Fig. 1). In the control samples B, D, and F, the carbon incorporation in the P δ-doping layer was avoided by inserting the buffer layer (right side of Fig. 1). In some samples, the carbon concentration appears to increase near the surface area, but this is mostly due to unavoidable carbon impurities on the SIMS sample surface.[29] In both samples with and without carbon structures, the segregation of P atoms towards the surface becomes more apparent with increasing growth temperature. However, the behaviors of P are appreciably different between the samples with and without interfacial carbon, especially when the results for the same growth temperature are compared. For the control samples B, D, and F (right side of Fig. 1), the concentration of P in capping layers drastically decreases with the increase of growth temperature. On the other hand, for samples A, C, and E with carbon (see left side of Fig. 1), the segregation of P is suppressed, and the sharp P distributions within a few nm are maintained below the growth temperature of 400 °C. In order to quantify the degree of segregation, we employ the segregation length, which is defined as the length from the peak to the concentration $1/e$. In Fig. 1, the slope near the peak of sample C (with carbon) is more abrupt than that of sample D (without carbon). Here the segregation length in sample C is estimated to be 1.6 nm, which is smaller than the 4.0 nm of Sb at 400 °C in Ge without carbon.[18] The segregation lengths are usually uniquely given for a given material at a given growth
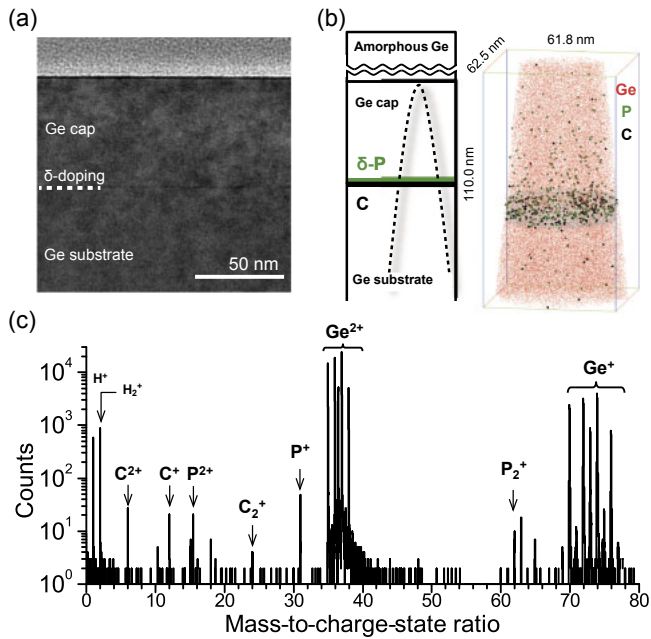
Fig. 2. (Color online) (a) XTEM image of sample A grown at 300 °C. The dashed line shows the interface between the capping layer and the substrate. (b) Schematic illustration of the sample structure. The dashed curve indicates the outline of the needle specimen for APT. Three-dimensional mapping of Ge, P, and carbon in Sample A is also shown. (c) Mass spectrum of the volume of $50\,\text{nm}\varphi \times 10\,\text{nm}$ [shown in (b)] around the P δ-doped and carbon-incorporated layers.

Fig. 3. (Color online) Room-temperature I–V characteristics for Au/Ti/n-Ge Schottky diode undoped and with P δ-doping. The inset shows the linear plot of I–V characteristics. For the undoped sample, the metal contact was fabricated directly on the substrate without P doping.

temperature, growth rate and substrate orientation, and hence, the length is uniquely determined under the same condition.[18–23] However, the present study shows successfully that such a characteristic can be changed drastically by the addition of an appropriate amount of carbon into Ge. Two different slopes are observed in the ranges of 0 to $-7\,\text{nm}$ and -10 to $-60\,\text{nm}$ in sample C. In the range of 0 to $-4\,\text{nm}$, the concentration of carbon is much higher than $10^{19}\,\text{cm}^{-3}$ and the P segregation is suppressed. In contrast, in the range of -10 to $-60\,\text{nm}$, where the carbon concentration is below $4 \times 10^{18}\,\text{cm}^{-3}$, the suppression of segregation is greatly weakened and the slope of the P concentration becomes small. In the range of -10 to $-60\,\text{nm}$, the gradient of the distribution of P in sample C becomes close to that for control sample D. We also investigate the effect of carbon using Ge(100) substrates and the same tendency is observed. Therefore this effect does not depend on crystal orientation. These results imply that in the high-concentration region of carbon, most of the carbon atoms remain at the growing surface and efficiently incorporate P atoms.

In order to investigate the crystal quality of the capping layer and the existence of other impurities, the interface between the substrate and the capping layer was inspected by TEM and APT. The TEM image of the sample grown at 300 °C (sample A) is shown in Fig. 2(a). The dashed line indicates the δ-doping position at the interface between the capping layer and the substrate. No dislocations were observed in the entire capping layer, indicating that high crystalline quality of the capping layer is obtained, although high concentrations of carbon and P exist at the interface. In addition, the impurity species at the interface were checked by APT. To apply APT to sample A, an additional amorphous Ge capping layer was deposited at room temper-

ature, as illustrated in Fig. 2(b), to protect the sample from Ga beam damage during focused ion beam irradiation for needle-specimen fabrication. In this figure, P and carbon distributions are shown in three-dimensional (3D) elemental mapping and elemental information on arbitrary regions can be extracted from the mapping. The mass spectrum around the P δ-doped and carbon-incorporated layers of sample A with a volume of $50\,\text{nm}\varphi \times 10\,\text{nm}$ is displayed in Fig. 2(c). Together with the peaks of mass-to-charge-state ratios (m/z) of doubly and singly positive Ge (Ge^{2+} and Ge^+) with the natural Ge isotopic ratios, the peaks of m/z at 15.5, 31, and 62, originating from P^{2+}, P^+, and P_2^+, respectively, were observed. In addition, carbon-related peaks of m/z at 6, 12, and 24 were clearly observed; however, no clear peaks from other impurities were seen. Therefore, P and carbon are the major impurities at the interface and other impurities are minor. The result indicates that P segregation is suppressed by the existence of carbon and the effect of other impurities can be excluded. Although the mechanism of the suppression is not yet clear, a new investigation is under way to observe the correlation between carbon and P atoms by APT.

### 3.2 Electrical characteristics for structures with carbon

Figure 3 shows the I–V characteristics of the Au/Ti/Ge capping/P delta doping/n-Ge structures that are undoped and doped with sheet density from 5×10^{13} to $5 \times 10^{14}\,\text{cm}^{-2}$ (samples G–I). Below $5 \times 10^{13}\,\text{cm}^{-2}$, rectifying behavior is observed owing to the Schottky barrier. With the increase in the P sheet density, the current on the reverse bias side increases significantly. For the samples having higher than $1 \times 10^{14}\,\text{cm}^{-2}$, Ohmic behaviors with low resistivity are obtained. It should be noted that such excellent Ohmic contact was obtained despite the coexistence of a large amount of carbon atoms near the P δ-doping layer. The electrical activation of the δ-doped P in the presence of carbon (samples H and I) was investigated by Hall measurements at 3 K and the results are summarized in Table II. Total (chemical) P sheet density was obtained by integrating the

Table II. Sheet density of dopants and carriers for the samples with and without carbon grown at various growth temperatures.

Growth temperature (°C)	Presence of carbon	Sheet density of dopants (10^{13} cm^{-2})	Sheet density of carriers (10^{13} cm^{-2})	Activation ratio (%)	Capping layer thickness (nm)
210[a]	No	24	4	17	22
250[a]	No	19	6.2	33	22
300[b]	Yes	8.8	2.9	33	15
300[c]	Yes	34	7.3	21	15
350[a]	No	15	7.2	48	22

a) Ref. [19]. b) Sample H. c) Sample I.

SIMS depth profiles, and a lower total P density than that deposited (Table I) is attributed to some experimental errors such as SIMS artifacts near the surface. At 3 K, the carriers in the substrates should freeze out, and hence, the carrier density obtained from Hall measurements represents that from δ-doped P. For comparison, the total P density and the carrier density for samples without carbon taken from Ref. [19] are also given in Table II. The carrier density of δ-doped P increases with increasing growth temperature because of the higher crystal quality of the capping layer.[19] It should be noted that the active carrier concentration of δ-doped P without carbon almost saturates above $\sim 10^{14}$ cm^{-2},[30] and that our results with carbon show a similar trend, as seen by comparing the result of sample H with that of sample I. The results in Table II show that the activation ratio of δ-doped P for the samples with carbon is comparable to those without carbon but is slightly lower. This slightly lower activation can be ascribed to the pre-annealing at 350 °C prior to the growth of the capping layer[19] and the deactivation of some P owing to the formation of complexes with carbon.[31] In order to investigate the effect of carbon on Ohmic behaviors, the I–V characteristics for P δ-doped samples with carbon were compared with those without carbon. Figure 4 shows the I–V characteristics for samples P δ-doped at 1×10^{14} cm^{-2} with and without carbon, where the buffer layer was uniformly and lightly ($\sim 10^{17}$ cm^{-3}) P-doped so that the layer is n-type. Schematics of the sample structures are shown at the top of Fig. 4. For the sample without carbon, the reverse current is higher than that for the undoped sample; however, a clear Ohmic contact is not obtained. On the other hand, for the sample with carbon, Ohmic behavior was clearly observed. This difference is attributable to the higher concentration region of P around the peak for sample A, where the carbon concentration is high enough to suppress the segregation of P. In diffusion processes, carbon reduces the diffusivity of the dopant by forming complexes, while a part of the dopants is inactive.[31] Here, the carbon contributes to the confinement of sufficiently high activated P dopants in the capping layer, resulting in the formation of Ohmic contacts, although some P can be deactivated by carbon. In samples J and K, the thickness of capping layers was further reduced to 5 and 3 nm, respectively (Fig. 5). Here sample J shows Ohmic behavior, while sample K with the 3-nm-thick capping layer shows the Schottky behavior. This is attributed to the decrease in the number of P atoms incorporated into the layer owing to the reduction of the capping layer thickness. Near the metal–semiconductor interface, the lower sheet density of electrically activated (ionized) dopants leads to a higher
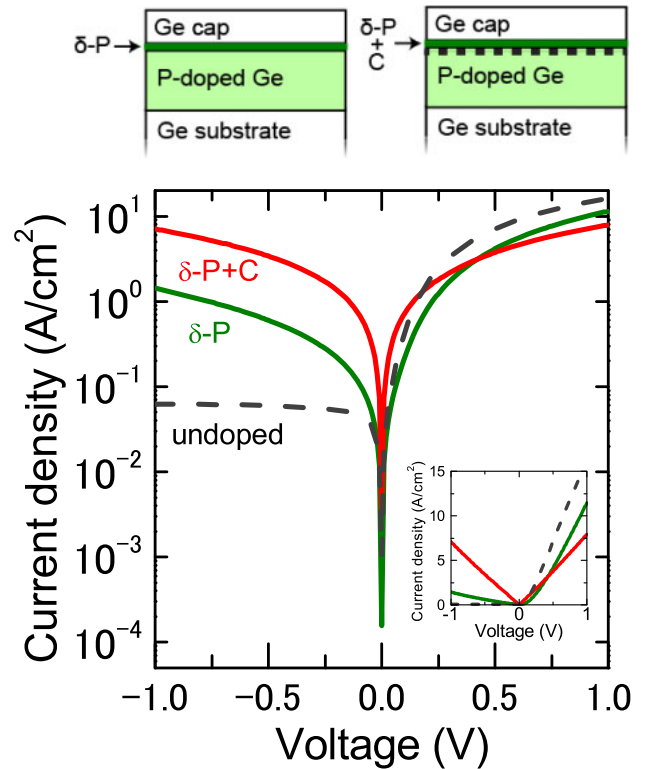
Fig. 4. (Color online) I–V characteristics for Au/Ti/n-Ge Schottky diodes which are undoped (dashed line) and P δ-doped at 1×10^{14} cm^{-2} with (red line) and without (green line) carbon. In order to measure I–V characteristics, the buffer layer was uniformly and lightly ($\sim 10^{17}$ cm^{-3}) P-doped so that the layer is n-type. The 15-nm-thick capping layers were grown at 300 °C. For the undoped sample, the metal contact was fabricated directly on the substrate without P doping.
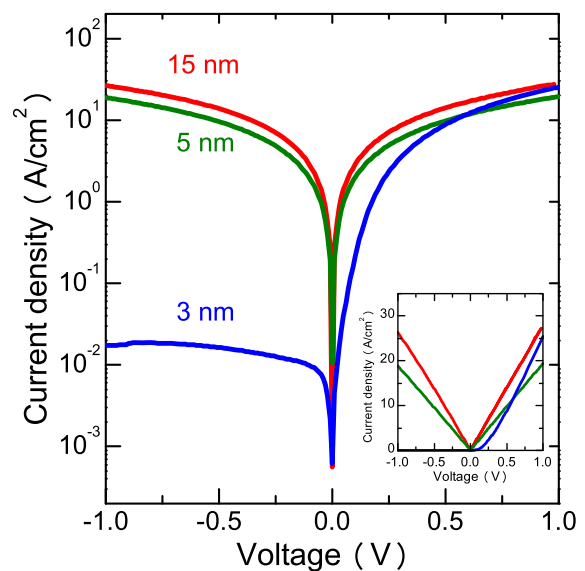
Fig. 5. (Color online) I–V characteristics for Au/Ti/n-Ge Schottky diode when the capping layer thickness was reduced from 15 to 3 nm. n-Ge was δ-doped at 1×10^{14} cm^{-2} at a growth temperature of 300 °C. The inset shows the linear plot of I–V characteristics.

effective barrier as a result of image-force lowering.[32] In addition, it has been reported that δ-doped P in silicon is not electrically active when the thickness of capping layers is less than 0.5 nm.[33] The P profile in the range of 0 to −7 nm is so steep that the 0.5-nm-thick inactive region can significantly

decrease active P atoms in the capping layer. This result indicates that the P atoms near the surface may not be electrically activated, and hence, sample K with the 3-nm-thick capping layer shows the Schottky behavior. P δ-doping with carbon insertion enables the formation of a much shallower junction compared with ion implantation.

4. Conclusions

We have demonstrated strong suppression of phosphorus segregation during the epitaxial growth of germanium upon the incorporation of carbon atoms. As a result, activated phosphorus donors with a sheet density of 2.9×10^{13} cm^{-2} confined within a few nm were obtained. The I–V measurements of such δ-doped layers showed excellent Ohmic behaviors, especially when the sheet density of phosphorus donors exceeded 1×10^{14} cm^{-2}. In addition, Ohmic behavior was observed when the capping layer was as thin as 5 nm. Moreover, the deposition of carbon atoms by methods such as the sublimation of graphite filaments enables the control of the carbon content and distribution.[34] These results indicate that P δ-doping with the incorporation of carbon is a useful technique for realizing an ultrashallow Ohmic contact on n-type Ge.

Acknowledgments

1) Y. Kamata, Mater. Today **11** [1], 30 (2008).
2) A. Dimoulas, P. Tsipas, A. Sotiropoulos, and E. K. Evangelou, Appl. Phys. Lett. **89**, 252110 (2006).
3) T. Nishimura, K. Kita, and A. Toriumi, Appl. Phys. Lett. **91**, 123123 (2007).
4) R. R. Lieten, S. Degroote, M. Kuijk, and G. Borghs, Appl. Phys. Lett. **92**, 022106 (2008).
5) Y. Zhou, M. Ogawa, X. Han, and K. L. Wang, Appl. Phys. Lett. **93**, 202105 (2008).
6) T. Nishimura, K. Kita, and A. Toriumi, Appl. Phys. Express **1**, 051406 (2008).
7) Y. Zhou, W. Han, Y. Wang, F. Xiu, J. Zou, R. K. Kawakami, and K. L. Wang, Appl. Phys. Lett. **96**, 102103 (2010).
8) M. Kobayashi, A. Kinoshita, K. Saraswat, H. S. P. Wong, and Y. Nishi, J. Appl. Phys. **105**, 023702 (2009).
9) P. P. Manik, R. K. Mishra, V. P. Kishore, P. Ray, A. Nainani, Y.-C. Huang, M. C. Abraham, U. Ganguly, and S. Lodha, Appl. Phys. Lett. **101**, 182105 (2012).
10) K. Ikeda, Y. Yamashita, N. Sugiyama, N. Taoka, and S. Takagi, Appl. Phys. Lett. **88**, 152115 (2006).
11) T. Nishimura, S. Sakata, K. Nagashio, K. Kita, and A. Toriumi, Appl. Phys. Express **2**, 021202 (2009).
12) M. Koike, Y. Kamimuta, E. Kurosawa, and T. Tezuka, Appl. Phys. Express **7**, 051302 (2014).
13) C. O. Chui, L. Kulig, J. Moran, W. Tsai, and K. C. Saraswat, Appl. Phys. Lett. **87**, 091909 (2005).
14) C. Wang, C. L. S. Huang, W. L. G. Yan, G. Lin, J. Wei, W. Huang, H. Lai, and S. Chen, Appl. Phys. Express **6**, 106501 (2013).
15) S. Brotzmann and H. Bracht, J. Appl. Phys. **103**, 033508 (2008).
16) M. Naganawa, Y. Shimizu, M. Uematsu, K. M. Itoh, K. Sawano, Y. Shiraki, and E. E. Haller, Appl. Phys. Lett. **93**, 191905 (2008).
17) E. Simoen and J. Vanhellemont, J. Appl. Phys. **106**, 103516 (2009).
18) K. Sawano, Y. Hoshi, K. Kasahara, K. Yamane, K. Hamaya, M. Miyao, and Y. Shiraki, Appl. Phys. Lett. **97**, 162108 (2010).
19) G. Scappucci, G. Capellini, and M. Y. Simmons, Phys. Rev. B **80**, 233202 (2009).
20) J. F. Nützel and G. Abstreiter, Phys. Rev. B **53**, 13551 (1996).
21) P. E. Thompson and G. G. Jernigan, Semicond. Sci. Technol. **22**, S80 (2007).
22) E. Friess, J. Nützel, and G. Abstreiter, Appl. Phys. Lett. **60**, 2237 (1992).
23) K. Nakagawa, M. Miyao, and Y. Shiraki, Thin Solid Films **183**, 315 (1989).
24) K. A. Bratland, Y. L. Foo, J. A. N. T. Soares, T. Spila, P. Desjardins, and J. E. Greene, Phys. Rev. B **67**, 125322 (2003).
25) G. M. Vanacore, M. Zani, G. Isella, J. Osmond, M. Bollani, and A. Tagliaferri, Phys. Rev. B **82**, 125456 (2010).
26) G. Lippert, H. J. Osten, D. Krüger, P. Gaworzewski, and K. Eberl, Appl. Phys. Lett. **66**, 3197 (1995).
27) D. E. Perea, E. R. Hemesath, E. J. Schwalbach, J. L. Lensch-Falk, P. W. Voorhees, and L. J. Lauhon, Nat. Nanotechnol. **4**, 315 (2009).
28) Y. Shimizu, H. Takamizawa, Y. Kawamura, M. Uematsu, T. Toyama, K. Inoue, E. E. Haller, K. M. Itoh, and Y. Nagai, J. Appl. Phys. **113**, 026101 (2013).
29) R. G. Wilson, F. A. Stevie, and C. W. Magee, *Secondary Ion Mass Spectrometry* (Wiley, New York, 1989) p. 2.4-1.
30) G. Mattoni, W. M. Klesse, G. Capellini, M. Y. Simmons, and G. Scappucci, ACS Nano **7**, 11310 (2013).
31) S. Brotzmann, H. Bracht, E. Simoen, E. E. Haller, J. S. Christensen, and P. Werner, Phys. Rev. B **77**, 235207 (2008).
32) S. M. Sze and K. K. Ng, *Physics of Semiconductor Devices* (Wiley, New York, 2006) 3rd ed., p. 134.
33) C. M. Polley, W. R. Clarke, J. A. Miwa, G. Scappucci, J. W. Wells, D. L. Jaeger, M. R. Bischof, R. F. Reidy, B. P. Gorman, and M. Simmons, ACS Nano **7**, 5499 (2013).
34) J. Kolodzey, P. A. O'Neil, S. Zhang, B. A. Orner, K. Roe, K. M. Unruh, C. P. Swann, M. M. Waite, and S. IsmatShah, Appl. Phys. Lett. **67**, 1865 (1995).